J Mater Sci (2011) 46:3928–3934
DOI 10.1007/s10853-011-5317-y

Investigations on green-emitting, Mn^{2+}: $BaAl_{12}O_{19}$ phosphors obtained by solution combustion process

Vijay Singh · R. P. S. Chakradhar · J. L. Rao · Ho-Young Kwak

Received: 3 September 2010 / Accepted: 22 January 2011 / Published online: 8 February 2011

Abstract Manganese-doped $BaAl_{12}O_{19}$ green phosphor was prepared using a self-propagating (combustion) synthesis. Powder X-ray diffraction and scanning electron microscopy were used to characterize the as-prepared combustion product. A room temperature photoluminescence study shows an emission line at 513 nm corresponding to a transition from the upper $^4T_1 \rightarrow {}^6A_1$ ground state of Mn^{2+} ions. The electron paramagnetic resonance (EPR) spectrum exhibits six line hyperfine structure at $g = 1.981$. From the EPR spectrum, the spin-Hamiltonian parameters have been evaluated. The g value indicates that the site symmetry around Mn^{2+} ions is distorted tetrahedral. The number of spins (N) participating in the resonance for $g = 1.981$ is measured as a function of temperature. The paramagnetic susceptibility (χ) is calculated from the EPR data at various temperatures. From the plot $1/\chi$ versus T, the Curie constant (C) and Curie paramagnetic temperature (θ_p) have been evaluated and discussed.

V. Singh (✉) · H.-Y. Kwak (✉)
Mechanical Engineering Department, Chung-Ang University, Seoul 156-756, Korea
e-mail: vijayjiin2006@yahoo.com

H.-Y. Kwak
e-mail: kwakh@cau.ac.kr

R. P. S. Chakradhar
Central Glass and Ceramic Research Institute, Kolkata 700032, India

J. L. Rao
Department of Physics, Sri Venkateswara University, Tirupati 517502, India

Present Address:
R. P. S. Chakradhar
CSIR-NAL, Bangalore 560 017, India

Introduction

Rare-earth and transition metal ions doped with alkaline earth aluminate oxide phosphor materials have been regarded as a potential candidate for various display devices such as flat panel displays, field emission displays, vacuum fluorescent displays, etc. due to their high efficiency, chemical stability, and high transparency in the visible range [1–4]. Among the alkaline earth aluminate oxides, Ba-hexa-aluminates doped with rare-earth ions have attained more and more attention because of their possible use in plasma display panels (PDPs), field emission displays (FEDs), and Hg-free lamps [1, 5, 6].

Manganese is an important transition metal ion, which has been used as activator in various luminescent materials. It is well documented that Mn^{2+}-doped phosphors can be effectively excited by many excitation sources such as UV-irradiation, X-ray and electric field, etc. [7–10]. Mn^{2+} emission in phosphor shows either in green or orange-to-red region [11, 12]. In general, octahedrally coordinated Mn^{2+} gives an orange to red emission whereas tetrahedrally coordinated Mn^{2+} gives a green emission [13]. It has been reported in the literature that another possibility to obtain a green Mn^{2+} emission is to choose a lattice in which Mn^{2+} is on a site which is considerably larger than the Mn^{2+} radius [14]. The concepts of energy transfer are not limited to rare-earth ions, rather it has also been observed in rare-earth and Mn^{2+} (transition metal) co-doped materials [15–17].

$BaAl_{12}O_{19}$:Mn represent a commercial green phosphor and is known to exhibit high luminous efficiency and good stability adaptable for plasma display panels (PDPs), field emission displays (FEDs), and possible new generation of Hg-free lamps [18, 19]. On the other hand, Zn_2SiO_4:Mn widely known for commercial green phosphor has a

relatively long decay time, which is disadvantage for its use as green source for PDPs [20]. Recently, the luminescence properties of divalent manganese ions have been studied intensively and are used in many luminescent materials [21–24]. However, luminescence studies in Mn^{2+}-doped $BaAl_{12}O_{19}$ are scant. Therefore, $BaAl_{12}O_{19}$:Mn phosphor has received much attention in recent years and is considered to be an alternative phosphor for potential applications. The aluminate of interest in the present study is Mn^{2+}-doped $BaAl_{12}O_{19}$ phosphor. Particularly, luminescence, from the 3d–3d transitions in Mn^{2+} ions, is strongly affected by the crystal field surrounding the luminescence center. Therefore, optical and electron paramagnetic resonance (EPR) spectra are ideal methods for studying the oxidation state and site of Mn in host lattices.

Recently, we have shown that, by combustion synthesis, aluminates can be synthesized at furnace temperature 500 °C within 5 min [25–28]. Elimination of secondary processing is a great advantage of combustion process. A similar method was adopted to produce manganese-doped $BaAl_{12}O_{19}$ phosphor, and manganese was incorporated as Mn^{2+} in $BaAl_{12}O_{19}$ host. The nature and structural details of the synthesized phosphor have been investigated by X-ray diffraction (XRD) and scanning electron microscopy (SEM) studies. The EPR and photoluminescence (PL) properties of this phosphor have also been studied. The EPR spectra were also recorded at different temperatures.

Materials and methods

$BaAl_{12}O_{19}$:Mn(0.02%) composition was synthesized by solution combustion method. High-purity $Ba(NO_3)_2$, $MnCl_2{\cdot}4H_2O$, $Al(NO_3)_3{\cdot}9H_2O$ and CH_6N_4O have been used as the starting materials. For complete combustion, the oxidizer/fuel ratio should be equal to 1. Stoichiometric amounts of starting materials were thoroughly mixed in a minimum volume of deionized water in a China dish. The dish was kept in a preheated furnace maintained at 500 ± 10 °C. Within a few minutes, the solution boiled and was ignited to produce a self-propagating flame. As soon as the reaction was over, dish was taken out and the foamy product is crushed into a fine powder and was used for characterization.

Powder XRD pattern was recorded using a Philips X' pert X-ray diffractometer with graphite monochromatized CuK_α radiation and nickel filter. Scanning electron micrographs (SEM) were taken using a JEOL-JSM-5610LV scanning electron microscope. The emission and excitation spectra were recorded at room temperature on a Hitachi F-4500 fluorescence spectrophotometer. EPR measurements were carried out using a Bruker EMX 10/12 X-band ESR spectrometer at various temperatures.

Results and discussion

X-ray diffraction

The powder diffraction pattern of the as-prepared $BaAl_{12}O_{19}$:Mn is shown in Fig. 1. The XRD pattern shows well-defined peaks, which indicates the crystallinity and phase formation of the synthesized compounds. The sample exhibits dominate diffraction peaks due to the hexagonal phase of $BaAl_{12}O_{19}$ (JCPDS, File-26-0135) along with weak $BaAl_2O_4$ and Al_2O_3 as a minor secondary phases. This should be noted that the crystallinity and hexagonal phase of $BaAl_{12}O_{19}$ could be obtained using urea-assisted combustion method even at furnace temperature 500 °C. It has been reported in the literature that pure hexagonal phase of $BaAl_{12}O_{19}$ is usually carried out at higher temperature (<1400 °C) as lower reaction temperatures produce $BaAl_{12}O_{19}$ with $BaAl_2O_4$ and Al_2O_3 impurities [29, 30].

The existence of hexa-aluminate $BaAl_{12}O_{19}$ was initially reported by Toropov [31]. Stevels [32] observed that the compound is nonstoichiometric, having a β-alumina-type structure with a broad composition, Ba_{1+x} $Al_{10.67}$ $+_{0.75x}$ O_{17+x} $(-0.2 \leq x \leq 0.35)$. Smets and Verlijsdonk [33] assumed the existence of two different hexa-aluminates with compositions of $1.29BaO{\cdot}6Al_2O_3$ and $0.82BaO{\cdot}6Al_2O_3$. The former was described as a β-alumina-type structure, while the latter was considered as having the same structure as the β-alumina type and close to the structure of $BaMgA_{l0}O_{17}$. More recently, it became clear that the hexa-aluminate spans a solid solution region, $xBaO{\cdot}6Al_2O_3$, where x extends from about 0.80 to 1.32, and there are two compounds of the β-alumina type [34–36].

The luminescence properties are closely related with the crystalline structure of host materials. The structure of $BaAl_2O_4$ is different and there are two different barium sites Ba(1) and Ba(2) [37–39]. Ba(1) and Ba(2) are positioned on 6c and 2a and coordinated by nine oxygen ions with average Ba–O distances of 2.97 for Ba(1) and 2.89 A for Ba(2). When Mn^{2+} ions are built into Ba sites, we expect that two Mn^{2+} emission centers existed in $BaAl_2O_4$:Mn^{2+}. The authors did not observe emission peaks corresponding to Ba(1) and Ba(2) sites of $BaAl_2O_4$:Mn^{2+}. On the other hand, Ba hexa-aluminate $BaAl_{12}O_{19}$ belong to space group $P63{=}mmc$ [40]. In general, tetrahedrally coordinated Mn^{2+} (weak crystal field) generates a green light; however, octahedrally coordinated Mn^{2+} (strong crystal field) gives an orange to red emission [41, 42].

Scanning electron microscopy

The surface morphology of the powder phosphor has been investigated by SEM. Figure 2 shows that typical SEM of

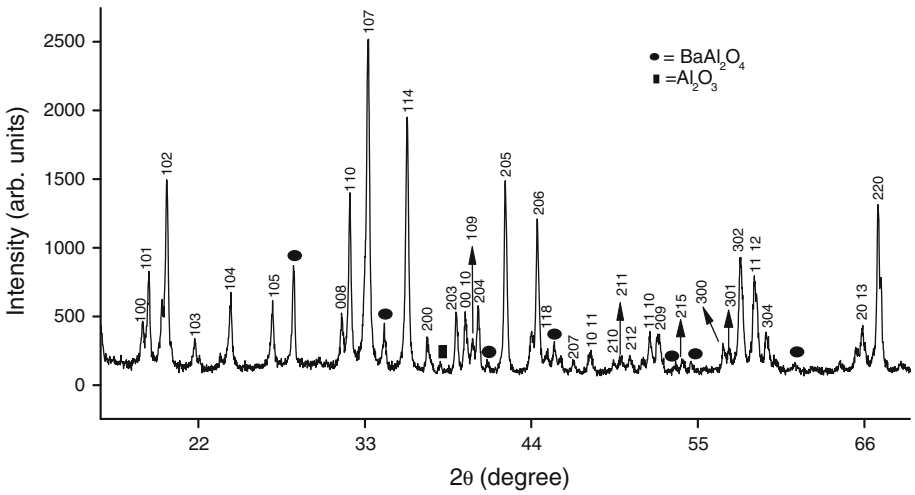

Fig. 1 XRD pattern of as-prepared $BaAl_{12}O_{19}$:Mn

the as-prepared $BaAl_{12}O_{19}$:Mn phosphor. Figure 2a shows that the particles are agglomerated and crystallite sizes are varying. The regularity in sizes and shapes may be due to the (i) non-uniform distribution of temperature and (ii) irregular mass flow during combustion. Combustion is also uncontrolled dynamic process. Also, porosity can be seen in the SEM micrographs. It is believed that the porosity is formed due to large amount of gases escaping during combustion reactions. Figure 2b is a magnified view of Fig. 2a (zone a) and c is a magnified view of Fig. 2b (zone b). From these high magnification images, it is clear that the powder products are highly fluffy with voids and pores. Also, the powder particle contains tiny crystals. The particle size cannot be measured exactly from the SEM.

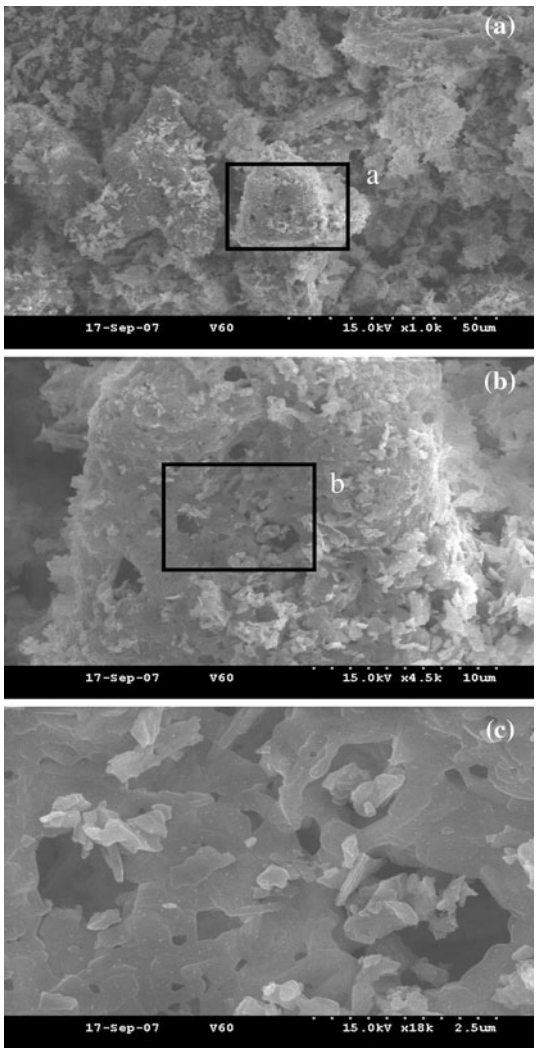

Fig. 2 SEM images of as-prepared $BaAl_{12}O_{19}$:Mn. **a** shows that the particles are agglomerated and crystallite sizes are varying. **b** is a magnified view of **a** (zone a) and **c** is a magnified view of **b** (zone b)

Electron paramagnetic resonance studies

Figure 3 shows the EPR spectra of $BaAl_{12}O_{19}$:Mn phosphor prepared by the combustion method. The EPR spectra of Mn^{2+} ions in this phosphors are commonly described by a spin-Hamiltonian [43]

$$H = ß\ \mathrm{B.g}\ .\mathrm{S} + \mathrm{D}\left[\mathrm{S}_z^2 - \{\mathrm{S}\ (\mathrm{S}+1)/3\}\right] + \mathrm{S.A.I} \quad (1)$$

The first term on right-hand side represents the electronic Zeeman term, the second term characterizes the zero-field splitting of the sextet ground state, and the last term represents the hyperfine coupling with the ^{55}Mn nuclei. It is observed that the EPR spectrum exhibited a well-resolved sextet hyperfine structure (hfs) centered at $g \approx 1.981$, due to interaction of electron spin with its own nuclear spin ($I = 5/2$) of ^{55}Mn [43–45]. The axial distortion of octahedral symmetry in case of d^5 transition metal ions gives rise to three Kramers doublets $|\pm 5/2\rangle$, $|\pm 3/2\rangle$, and $|\pm 1/2\rangle$ [43]. Application of Zeeman field splits the spin

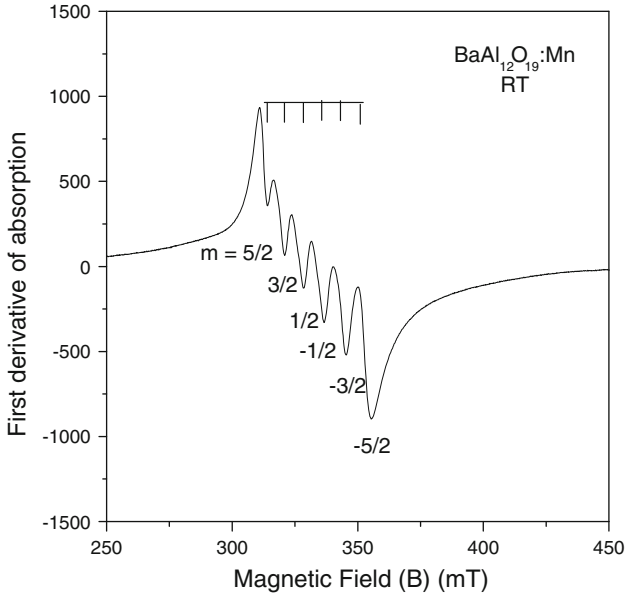

Fig. 3 EPR spectrum of $BaAl_{12}O_{19}$:Mn phosphor at room temperature

degeneracy of the Kramers doublets. As the crystal field splitting is normally much smaller than the Zeeman field, the resonances observed are due to transitions within the Kramers doublets. The observed sextet arises from the Ms $= -1/2$ to $+1/2$ transition. The magnitude of hyperfine splitting constant (A) and the green emission are the key factors for assigning the ESR sextet to a tetrahedral Mn^{2+} ion. It is reported that both in octahedral (Oh) and tetrahedral (Td) symmetry, Mn^{2+} ions exhibit a sextet hyperfine (hfs) centered at $g \sim 2.0$ [46–48]. The hyperfine splitting constant (A) is one of the parameters to make clear the coordination number of Mn^{2+} ions in various samples, which depends on the host matrices and their crystallinity. In general, A values for Oh coordinated compounds are $\sim$100 gauss [47], and for Td coordinated compound $\sim$83 gauss [48]. In this study, the authors observed A value of 84 gauss which indicates that Mn^{2+} ions are in Td symmetry. As mentioned earlier, it is has been reported in literature, that the tetrahedrally coordinated Mn^{2+} ions give a green emission, whereas octahedrally coordinated Mn^{2+} ions give an orange to red emission [41]. In this study, the authors have observed a green emission peak, at 513 nm in their photoluminescence studies which also confirms that Mn^{2+} ions are in T_d symmetry.

The ability to observe the ^{55}Mn hyperfine structure at $g \approx 1.981$ has two tangible benefits: (1) It generally allows unambiguous assignments of positions of complex resonance lines to manganese; and (2) The magnitude of hyperfine splitting (hfs) constant provides a measure of bonding between Mn^{2+} ion and its surrounding ligands [49, 50]. This means a qualitative measure of the covalency of the bonding in the matrix which can be determined from the value of A; the smaller the splitting, the more covalent the bonding of the anion. Van Wieringen [49] empirically determined a positive correlation between 'A' and the ionicity of the manganese–ligand bond. In this study, the observed 'A' value is $\approx$84 G which indicates that the Mn^{2+} ions are in a moderately in covalent environment. It is also observed that the line width, g and A values are found to be independent of temperature.

The number of spins participating in resonance can be calculated by comparing the area under the absorption curve with that of a standard ($CuSO_4{\cdot}5H_2O$ in this study) of known concentration. Weil et al. [51] gave the following expression which includes the experimental parameters of both sample and standard.

$$N = \frac{A_x(\mathrm{Scan}_x)^2 G_{\mathrm{std}}(B_m)_{\mathrm{std}}(g_{\mathrm{std}})^2[S(S+1)]_{\mathrm{std}}(P_{\mathrm{std}})^{1/2}}{A_{\mathrm{std}}(\mathrm{Scan}_{\mathrm{std}})^2 G_x(B_m)_x(g_x)^2[S(S+1)]_x(P_x)^{1/2}}[\mathrm{Std}] \quad (2)$$

where A is the area under the absorption curve which can be obtained by double integrating the first derivative EPR absorption curve, Scan is the magnetic field corresponding to unit length of the chart, G is the gain, B_m is the modulation field width, g is the g factor, S is the spin of the system in its ground state, and P is the power of the microwave. The subscripts "x" and "std" represent the corresponding quantities for Mn^{2+} in $BaAl_{12}O_{19}$ phosphor and the reference ($CuSO_4{\cdot}5H_2O$), respectively. The number of spins participating in resonance at $g \approx 1.981$ has been calculated at room temperature as well as at different low temperatures. Figure 4 shows a plot of logarithmic dependence of the number of spins (log N) participating in resonance versus the reciprocal of absolute temperature ($1/T$). From the plot, it is seen that as the temperature is lowered, the population of spin levels increases, and a linear relationship is observed between log N and $1/T$, obeying the Boltzmann law. The data have been a least square fit to a straight line $\log N = 19.49 + (67.38/T)$.

The paramagnetic susceptibilities have been calculated by making use of the number of spins at different temperatures using the expression [52]

$$\chi = \frac{Ng^2\beta^2 J(J+1)}{3k_B T} \quad (3)$$

where N is the population of spin levels/kg, g is spectroscopic splitting factor, β is the Bohr magneton, k_B is the Boltzmann constant, and $J = 5/2$. The N can be calculated from (Eq. 2), and g has been taken from EPR data. From Fig. 5, it is evident that with increasing temperature, the susceptibility of the sample decreases obeying the Curie–Weiss law. The data are fit to a straight line in accordance

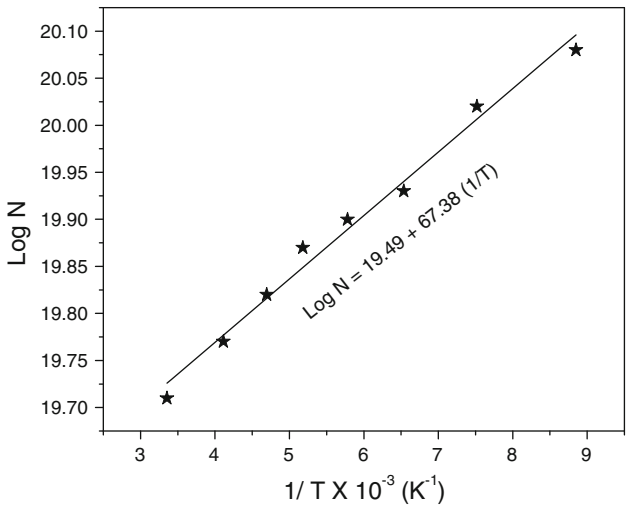

Fig. 4 A plot of logarithmic intensity (Log N) versus $1/T$ for $BaAl_{12}O_{19}$:Mn phosphor

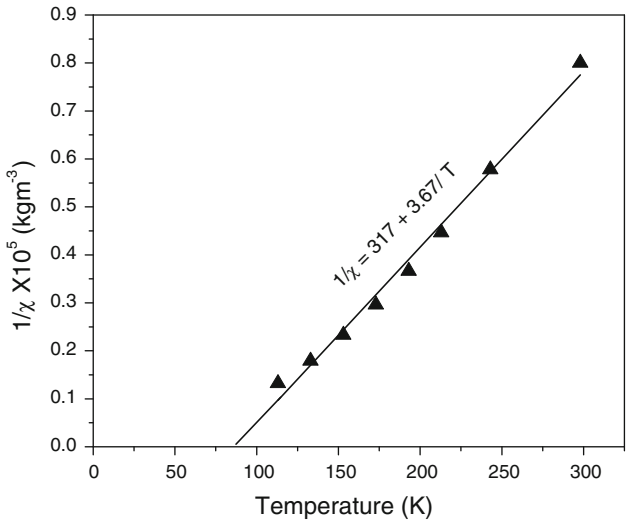

Fig. 5 The variation of reciprocal of paramagnetic susceptibility $1/\chi$ as a function of temperature (T) for $BaAl_{12}O_{19}$:Mn phosphor

with Curie–Weiss-type behavior. From the fit, the Curie constant (C) and paramagnetic Curie temperature (θ_p) have been evaluated, and are found to be 0.272 emu/mol and $\theta_p = 87$ K, respectively. It has been reported in the literature that, at low temperatures, if the paramagnetic Curie temperature is negative, then magnetic ions are antiferromagnetically coupled, whereas if it positive, then it is ferromagnetically coupled. In this study, the evaluated Curie temperature ($\theta_p = 87$ K) indicates that the Mn^{2+} ions are ferromagnetically coupled. The observed Curie constant and Curie temperature values obtained in this study are in good agreement with the values reported for paramagnetic ion.

Photoluminescence studies

The photoluminescence properties $BaAl_{12}O_{19}$:Mn phosphor has been characterized by the transition of $3d^5$ electrons in the manganese ion acting as an activating center. Mn^{2+} (d^5) gives rise to free ion terms ^6S, ^4P, ^4F, and ^4G, in addition to a number of doublet states of which ^6S is the ground state. In crystal fields, ^6S and ^4P transform as $^6A_1$ and $^4T_1$, respectively. ^4D and ^4G split into $^4E + {}^4T_2$ and $^4A_1 + {}^4E + {}^4T_1 + {}^4T_2$, respectively. Figure 6(a) shows the excitation spectrum, and Fig. 6(b) emission spectrum of $BaAl_{12}O_{19}$:Mn phosphor prepared by the combustion method. The excitation spectrum consists of five bands at 279, 360, 386, 427, and 452 nm characteristic of Mn^{2+} ions in tetrahedral symmetry, and the observed excitation peaks are due to transitions from the ground state $^6A_1$ (S) to excited states of $^4A_2$ (F), ^4E (D), $^4T_2$ (D), $^4A_1$ (G): ^4E (G), and $^4T_2$(G), respectively of Mn^{2+} ions.

The luminescence of $BaAl_{12}O_{19}$:Mn exhibits a green emission peak around 513 nm (Fig. 6(b)) from the synthesized phosphor upon excitation of 452 nm. The luminescence is assigned to a transition from the upper $^4T_1 \rightarrow {}^6A_1$ ground state of Mn^{2+} ions which is directly responsible for green light emission [53, 54]. This transition is doubly forbidden in terms of spin and parity selection rules so that a relatively slow decay process could be expected. Recently, Jun Zhou et al. [55] prepared $BaAl_{12}O_{19}$:Mn phosphor by flux-assisted (H_3BO_3) solid-state reaction method and studied their photoluminescence properties. They observed a broad band green emission at 517 nm upon VUV excitation (147 nm). Their results showed that the intensity of emission is enhanced by

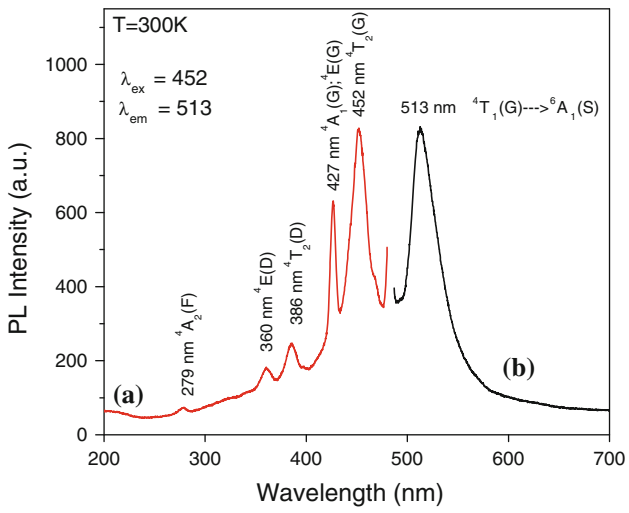

Fig. 6 Photoluminescence spectra of the: as-prepared $BaAl_{12}O_{19}$:Mn phosphor (a) excitation spectrum ($\lambda_{em} = 513$ nm) and (b) emission spectrum ($\lambda_{ex} = 452$ nm)

adding 7 wt% of H_3BO_3 as flux compared to that without flux. In this study, the Mn^{2+} ion substitutes for Al^{3+} in the $BaAl_{12}O_{19}$ lattice due to similar ionicity. There are three different kinds of tetrahedrally coordinated Al^{3+} sites in $BaAl_{12}O_{19}$ which are adoptable for Mn^{2+} emitting green light, but Mn^{2+} preferentially enters tetrahedral Al(2) sites of $BaAl_{12}O_{19}$ which has two Al(2) sites with a distance about 0.34 nm between them [42]. The Mn^{2+} ion in $BaAl_{12}O_{19}$ has fourfold coordination since it replaces Al^{3+} in the host, and hence the green emission occurs.

Conclusions

Using metal nitrates, and carbohydrazide as the starting materials, $BaAl_{12}O_{19}$:Mn phosphor was successfully synthesized by solution combustion processing at relatively low temperature (500 °C). Hexagonal phase of $BaAl_{12}O_{19}$ could be obtained by this method even at furnace temperature 500 °C with weak $BaAl_2O_4$ and Al_2O_3 as minor secondary phases. SEM results show that rough surface of the powder with voids and pores. The EPR spectrum exhibits a six-line hyperfine structure at $g \approx 1.981$. The resonance at $g \approx 1.981$ is due to Mn^{2+} ions in an environment close to tetrahedral symmetry and is known to arise from the transition between the energy levels of the lower doublet $|\pm 1/2\rangle$. The hyperfine value suggests that the Mn^{2+} ions are in a moderately covalent environment. It is also observed that the line width, g, and A values are found to be independent of temperature. It is observed that as the temperature is lowered, the population of spin levels increases, and a linear relationship is observed between log N and $1/T$, obeying the Boltzmann law. The variation of susceptibility of the sample with temperature obeys Curie–Weiss law. The Curie temperature ($\theta_p = 87$ K) indicates that the Mn^{2+} ions are ferromagnetically coupled at low temperatures. The luminescence at 513 nm is assigned to a transition from the upper $^4T_1 \rightarrow {}^6A_1$ ground state of Mn^{2+} ions which is directly responsible for green light emission.

Acknowledgements The first author VS expresses his thanks to the Hanse-Wissenschaftskolleg (Delmenhorst, Germany) for the research fellowship. VS is also grateful to the Chung-Ang University, Seoul (South Korea) for providing the Research Assistant Professorship under BK21 program. Dr. RPSC is grateful to Dr. H. S. Maiti, Director, CGCRI, and Dr. R. Sen, Head, GTL lab, CGCRI for their constant support and encouragement throughout this research.

References

1. Yokota K, Zhang S-X, Kimura K, Sakamoto A (2001) J Lumin 92:223
2. Jüstel T, Bechtel H, Mayr W, Wiechert DU (2003) J Lumin 104:137
3. Xing D-S, Gong M-L, Qiu X-Q, Yang D-J, Cheah K-W (2006) Mater Lett 60:3217
4. Chao L, Chao Z, Yan D, Tong C, Jianqing J, Jinhua H (2006) J Rare Earths 24:153
5. Sohn KS, Park FS, Kim CH, Park HD (2000) J Electrochem Soc 147(11):4368
6. Lee SH, Koo HY, Jung DS, Yi JH, Kang YC (2009) Ceram Int 35:2651
7. Bonder V, Axelrud L, Davydov V, Felter T (2001) Mater Res Soc Symp Proc 639:G11.36.1
8. Williams GVM, Schweizer S, Henke B, Dunford C, Edgar A (2006) Curr Appl Phys 6:351
9. Zhang X, Zeng H, Su Q (2007) J Alloys Compd 441:259
10. Hao Y, Wang Y (2007) J Lumin 122–123:1006
11. Wang X-J, Jia D, Yen WM (2003) J Lumin 102–103:34
12. Hernández JA, Camarillo EG, Muñoz G, Flores CJ, Cabrera EB, Jaque F, Romero JJ, García Solé J, Murrieta HS (2001) Opt Mater 17:491
13. Palumbo DT, Brown JJ Jr (1970) J Elctrochem Soc 117:1184
14. Koskentalo T, LeskelI M, Niinist L (1985) Mater Res Bull 20:265
15. Chen W, Li GH, Malm J (2000) J Lumin 91:141
16. You H, Song Y, Jia G, Hong G (2008) Opt Mater 31:342
17. Lu SW, Lee BI, Wang ZL (2001) J Lumin 92:76
18. Pike V, Patraw S, Diaz AL, Deboer BG (2003) J Solid State Chem 173:359
19. Kang YC, Chung YS, Park SB (1999) J Mater Lett 18:779
20. Rona C (1997) J Lumin 72–72:49
21. Kwon MS, Kim CJ, Park HL, Kim TW, Lee HS (2005) J Mater Sci 40:4089. doi:10.1007/s10853-005-0794-5
22. Kim CJ, Kwon MS (2006) J Mater Sci 41:6138. doi:10.1007/s10853-006-0423-y
23. Singh SP, Chakradhar RPS, Rao JL, Karmakar B (2010) Physica B 405:2157
24. Ye S, Zhang J, Zhang X, Wang X (2007) J Lumin 122–123:914
25. Singh V, Chakradhar RPS, Rao JL, Kim D-K (2007) J Solid State Chem 180:2067
26. Singh V, Natarajan V, Zhu J-J (2007) Opt Mater 30:468
27. Singh V, Gundu Rao TK, Zhu J-J (2008) J Lumin 128:583
28. Singh V, Gundu Rao TK (2008) J Solid State Chem 181:1387
29. Kimura S, Bannai E, Shindo I (1982) Mater Res Bull 17:209
30. Wang YH, Li F (2007) J Lumin 122–123:866
31. Toropov NA, Nauk DA (1935) SSSR 6:147
32. Stevels ALN (1978) J Lumin 17:121
33. Semts BMJ, Verlijsdonk JG (1986) Mater Res Bull 21:1305
34. Smets B, Rutten J, Hoeks G, Verlijsdonk J (1989) J Electrochem Soc 136:2119
35. Gobels M, Kimura S, Woermann E (1998) J Solid State Chem 136:153
36. You H, Zhang J, Hong G, Zhang H (2007) J Phys Chem C 111:10661
37. Horkner VW, Muller-Bschbaum H, Anorg Z (1979) Allg Chem 451:40
38. Haung S, Von Der Muhll R, Ravez J, Chaminade J, Hagenmuller P, Couzi M (1994) J Solid State Chem 109:97
39. Rodehorst U, Carpenter M, Marion S, Henderson C (2003) Mineral Magn 67:989
40. Iyi N, Inouse Z, Takekawa S, Kimura S (1984) J Solid State Chem 52:66
41. Blasse G, Grabmaier BC (1994) Luminescent materials. Springer-Verlag, Berlin
42. Bellotto M, Artioli G, Cristiani C, Forzatti P, Groppi G (1998) J Catal 179:597
43. Abragam A, Bleaney B (1970) Electron paramagnetic resonance of transition ions. Clarendon, Oxford
44. Fuxi G (1992) Optical and spectroscopic properties of glass. Springer, Berlin (chapter 6)

45. Misra SK (1996) Appl Magn Reson 10:193
46. Kim JS, Kim JS, Kim TW, Kim SM, Park HL (2005) Appl Phys Lett 86:091912
47. Franco RWA, Lima JF, Magon CJ, Donoso JP, Messaddeq Y (2006) J Non-Cryst Solids 352:3414
48. Sanada T, Yamamoto K, Wada N, Kojima K (2006) Thin Solid Films 496:169
49. van Wieringen JS (1955) Discuss Faraday Soc 19:118
50. Tsay FD, Helmholz L (1969) J Chem Phys 50:2642
51. Weil JA, Bolton JR, Wertz JE (1994) Electron paramagnetic resonance-elementary theory and practical applications. Wiley, New York, p 498
52. Aschcroft NW, Mermin ND (2001) Solid state physics. Harcourt College Publishers, Fort Worth, TX, p 656
53. Stevels ALN, Vink AT (1974) J Lumin 8:443
54. Robbins DJ, Mendez EE, Giess EA, Chang IF (1984) J Electrochem Soc 131:141
55. Zhou J, Wang Y, Liu B, Lu Y (2009) J Alloys Compd 484:439